applied sciences

MDPI

Article

Comparison between Eight-Axis Articulated Robot and Five-Axis CNC Gantry Laser Metal Deposition Machines for Fabricating Large Components

Simone Maffia [1,*], Federico Chiappini [2], Gianluca Maggiani [2], Valentina Furlan [1], Massimo Guerrini [2] and Barbara Previtali [1]

[1] Department of Mechanical Engineering, Politecnico di Milano, Via La Masa 1, 20156 Milan, Italy
[2] Nuovo Pignone Tecnologie S.r.l., Baker Hughes, Via Felice Matteucci 2, 50127 Florence, Italy
* Correspondence: simone.maffia@polimi.it

Featured Application: Laser metal deposition of large axisymmetric components.

Abstract: Laser metal deposition (LMD) is an additive manufacturing (AM) process capable of producing large components for the aerospace and oil and gas industries. This is achieved by mounting the deposition head on a motion system, such as an articulated robot or a gantry computer numerical control (CNC) machine, which can scan large volumes. Articulated robots are more flexible and less expensive than CNC machines, which on the other hand, are more accurate. This study compares two LMD systems with different motion architectures (i.e., an eight-axis articulated robot and a five-axis CNC gantry machine) in producing a large gas turbine axisymmetric component. The same process parameters were applied to both machines. The deposited components show no significant differences in geometry, indicating that the different performances in terms of accuracy of the two machines do not influence the outcome. The findings indicate that LMD can consistently produce large-scale axisymmetric metal components with both types of equipment. For such an application, the user has the option of using an articulated robot when flexibility and cost are essential, such as in a research context, or a CNC machine where ease of programming and process standardization are important elements, such as in an industrial environment.

Keywords: laser metal deposition; directed energy deposition; articulated robot; gantry computer numerical control machine; large components; 3D scans

Citation: Maffia, S.; Chiappini, F.; Maggiani, G.; Furlan, V.; Guerrini, M.; Previtali, B. Comparison between Eight-Axis Articulated Robot and Five-Axis CNC Gantry Laser Metal Deposition Machines for Fabricating Large Components. *Appl. Sci.* **2023**, *13*, 5259. https://doi.org/10.3390/app13095259

Academic Editors: Giada Gasparini and Vittoria Laghi

Received: 20 March 2023
Revised: 20 April 2023
Accepted: 21 April 2023
Published: 23 April 2023

1. Introduction

The sustainable energy transition is currently one of the major challenges that are being addressed by the global scientific and industrial community. This requirement is pushing the development of novel solutions, such as the digitalization of industrial processes and the use of smart technology, with the goal of reducing material and energy waste [1]. Under these conditions, additive manufacturing (AM) in all of its forms is gaining popularity in a variety of fields because it allows for a significant reduction in required and wasted material through a variety of means, ranging from stock material reduction to the realization of free form topologically optimized components, due to the ability of these technologies to add material only where needed [2]. Eliminating unnecessary material from components is especially beneficial in industries where weight savings are essential, such as in the aerospace sector [3]. Furthermore, the optimized supply chain of AM technologies (i.e., the absence of molds and the ability to easily realize one-of-a-kind parts) is a notable feature in the oil and gas sector, where very small batches of large components (typically realized by forging or casting) are common and a short lead time is frequently required [4].

Laser metal deposition (LMD) is an additive manufacturing process that uses thermal energy, specifically a laser beam, to melt the metal precursor (in the form of wire or powder)

as it is supplied to the deposition area, resulting in a molten pool of liquid metal [5]. The mutual motion of the laser beam and the fed material on a tool path generated by CAM software on the base of a CAD file realizes the solid component. With LMD, high deposition rates are available, and support-free near-net shape components can be realized, making it an excellent option for technological transition in areas such as aerospace, oil and gas, and construction [6]. The ability to manufacture large components is related to the fact that the deposition head is mounted on a motion system that moves it, and it follows the defined tool path to realize the part. This motion system can be a robot or a computer numerical control (CNC) machine with multiple degrees of freedom [7,8].

The choice between one motion system and the other may be difficult because of the many differences between the two configurations. In general, robots are more flexible than CNC machines because they have more degrees of freedom and may be used for a variety of tasks, but they are less accurate and precise (especially from the point of view of the trajectory between points) [9]. Robots have inferior geometrical accuracy and precision due to their extended cantilever kinematic structure, which must support the motors, brakes, and reduction gears of each axis, whereas the axes of cartesian CNC machines are stiffer and more robust and less influenced by vibrations [10]. Differences in the kinematic architecture of the two explored configurations lead to variations in trajectory and travel speed management. Indeed, due to the complicated kinematic chain of articulated robots, they may struggle to maintain the specified linear path with the given travel speed, resulting in a trajectory approximation or travel speed fluctuation [11]. This fact, when considered in the context of the discussed application, may result in the realization of inaccurate geometries as a result of an incorrect tool path or material shortage or accumulation as a result of speed increments or decrements, respectively [12–14]. CNC cartesian machine architectures, on the other hand, are isotropic in all reachable points and do not suffer from this issue. Because of this, machine builders typically propose LMD machines with CNC cartesian kinematics instead of articulated robot-based machines [15]. However, one major drawback is the increased cost of such systems, which can be about ten times more expensive than articulated robots [16]. For this reason, it is common to see articulated robot-based LMD machines used for research purposes. The high cost of the machine implies the high cost of the finished product, making LMD not always economically advantageous in some instances, and this is likely to keep the technology from spreading [17].

This debate applies not only to metal additive manufacturing but also to other technologies. Moreover, the topic is often debated in the construction research field, where huge volumes of deposition are ordinary. The primary AM technologies used in the construction industry include wire arc AM (WAAM) for metallic structures [18,19] and concrete deposition for 3D-printed buildings [20,21]. One of the research questions addressed is the selection between CNC gantry and articulated robot machines. The former often come larger in size than robots, and their actual dimensions determine the available build volume. Articulated robots are smaller, but the theoretical build volume is nearly endless because robots may be placed on movable platforms and moved around, despite higher geometrical uncertainty [22–24]. Fused deposition modeling (FDM) is another AM technology that is commonly employed in large constructions. Polymer extrusion methods, which are typically used in the manufacturing of freeform organic shapes and big design elements, are the ones that benefit the most from robot free-form flexibility [25,26]. Finally, the benefits of using a robot for tool manipulation are being researched for subtractive manufacturing methods, too, such as milling and drilling operations [27]. In fact, the machining sector is looking to robots for their flexibility, multi-purpose and large-scale capabilities, and reduced cost when compared to CNC machines. Yet, due to the physical interaction between the machined component and the tool, which must apply a force to remove the material, concerns regarding the low precision and stiffness of industrial robots are much more felt [10,11].

As a result, while the theoretical benefits and drawbacks of utilizing an articulated robot instead of a CNC machine for AM purposes are recognized, they have yet to be

examined in LMD applications. A case study from the oil and gas industry is provided in this article, and multiple aspects are addressed. A large-scale axisymmetric component of a gas turbine was chosen for fabrication on two LMD machines: one with an articulated robot and one with a CNC gantry. In terms of the laser source, optics, and powder management configurations, the two machines have almost identical setups. The geometrical accuracy of the two machines is analyzed by comparing the two realized components to the original CAD file using 3D scanning techniques, and by comparing the two scans with each other, the performances of the two machines can be evaluated. In the end, the two deposited parts did not show any remarkable differences in their geometry, assessing that both the tested kinematics configurations are suitable for realizing large-scale axisymmetric components with comparable accuracy. Indeed, the chosen geometry is representative of many components related to the oil and gas field, making the results applicable not only to the specific case study but to a whole family of parts. In conclusion, when large-scale axisymmetric components are considered, the users have the freedom of selecting the best solution for their needs without bothering about the geometrical accuracy performances of the machine. An articulated robot system should be considered when flexibility and cost reduction are preferred, and CNC gantry or cartesian machines should be preferred while robustness and easiness of programming are necessary.

2. Materials and Methods

2.1. Powder and Substrates

For the experiments, AP&C–GE Additive (Saint Eustache, QC, Canada) plasma atomized IN718 powder was used. The chemical composition of the powder conforms to the ASTM B637 (grade UNS N07718) standard [28]. Figure 1 is an SEM image of the powder. Because of the plasma atomization process, the particles are extremely round and smooth. The nominal powder granulometry ranges from 25 to 45 µm. The particle size distribution of the utilized powder was measured using a Morphologi 4 optical particle size analyzer from Malvern Panalytical Ltd. (Malvern, UK). Figure 2 depicts the outcome. Stainless steel AISI 304 substrates with dimensions of 400 × 400 × 30 mm were used for the experiments.

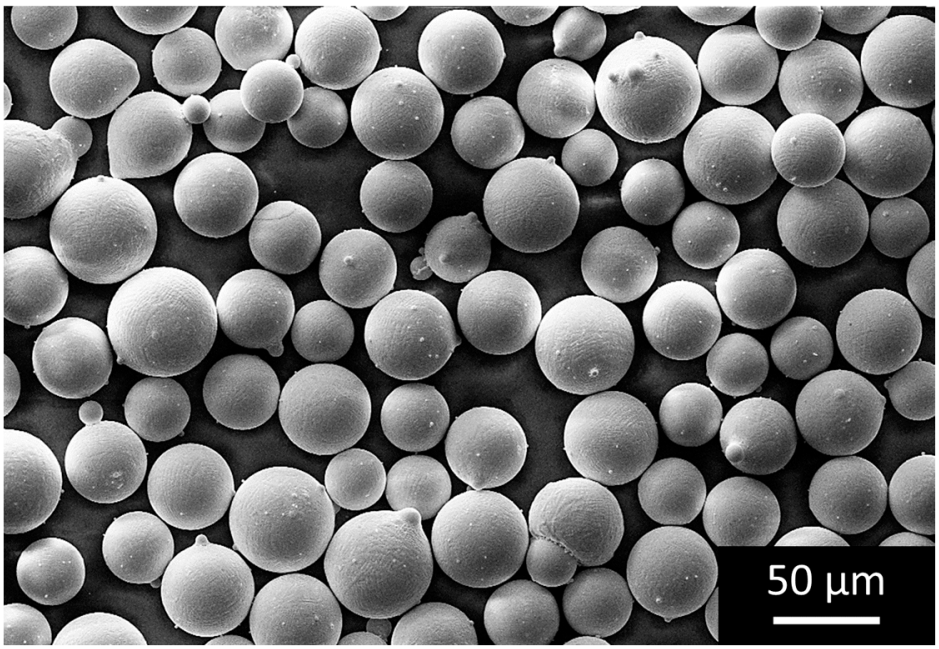

Figure 1. SEM image of the used IN718 powder.

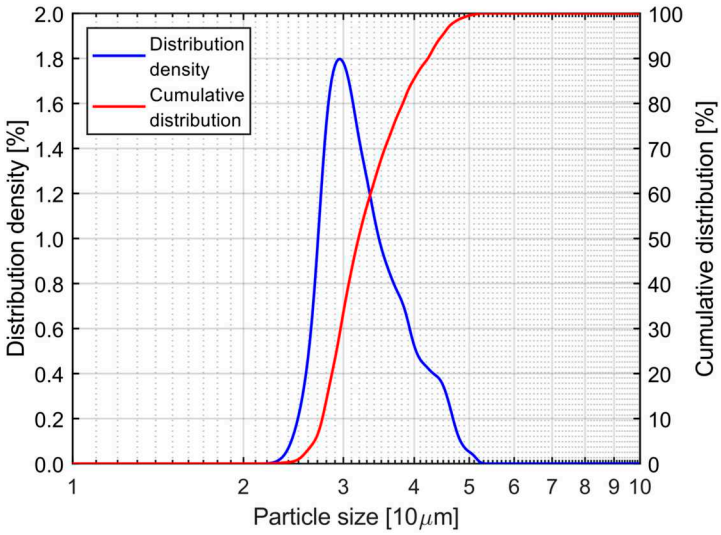

Figure 2. Particle size distribution of the used IN718 powder.

2.2. Description of the Two Tested LMD Machines

This study evaluates and compares an articulated robot-based LMD machine by BLM GROUP (Cantù, Italy) and a CNC gantry-based LMD machine by SM Systems S.r.l. (Torre Canavese, Italy). The two machines are very similar in terms of laser source, optical, and powder feeding settings; however, they differ significantly in terms of kinematic arrangement, maximum build size, and weight. The technical information on the two systems is summarized in Table 1. Figures 3 and 4 show the two machines.

Table 1. Summary of the characteristics and properties of the two machines.

	Machine Manufacturer	**BLM GROUP**	**SM SYSTEMS**
Laser source	Model	IPG YLS-3000	IPG YLS-4000
	Wavelength, [nm]	1070	1070
	Max power, [W]	3000	4000
Feeding fiber	Core diameter, [μm]	100	100
Process fiber	Core diameter, [μm]	400	600
Deposition head	Model	Kuka MWO-I-Powder	Kuka MWO-I-Powder
	Collimating lens focal length, [mm]	129	129
	Focusing lens focal length, [mm]	200	200
Laser beam characteristics	Beam parameter product, *BPP* [mrad·mm]	14.1	21.3
	Quality factor, M^2 [–]	41.8	62.5
Powder nozzle	Model	Fraunhofer ILT COAX-40-F	Fraunhofer ILT COAX-40-F
Powder feeder	Model	GTV TWIN PF 2/2-MF	Sulzer TWIN 10 C
	Working principle	Rotary disk	Rotary disk
Motion system	Kinematics configuration	Articulated robot + positioner	Gantry system + positioner
	Number of axes	6 + 2 (rotation + tilting)	3 + 2 (rotation + tilting)
	Repeatability, [mm]	0.03	0.01

Both machines are equipped with an IPG Photonics (Oxford, MI, USA) high power continuous wave Ytterbium active fiber laser source that generates a laser beam with a wavelength of 1070 nm. The maximum output power of the two sources, however, differs: 3000 W for the robot-based machine and 4000 W for the gantry-based machine. The laser beam is delivered from the laser source to the deposition head in the same way in both machines via a feeding fiber and a process fiber connected by a fiber-to-fiber

coupler. The feeding fiber core diameter in both machines is 100 µm, while the process fiber core diameter in the robot-based and gantry-based machines is 400 µm and 600 µm, respectively. Both machines are outfitted with a KUKA AG MWO I Powder deposition head (Augsburg, Germany). The focal lengths of the collimating and focusing lenses of this model of deposition head are 129 mm and 200 mm, respectively. Manipulation of the position of the focal point of the laser along the optical axis is accomplished by adjusting the distance between the collimation lens and the process fiber outlet. Thanks to this feature, the two machines can function with the same laser spot diameter on the working plane even though their process fibers have different core diameters. The beam parameter product BPP and the quality factor M2 at the outlet of the deposition head are 14.1 mrad·mm and 41.8 mrad·mm for the robot base system, respectively, and 21.3 mrad·mm and 62.5 for the gantry-based system.

On both machines, a Fraunhofer ILT COAX 40 F powder nozzle (Aachen, Germany) was employed. The two powder feeders mounted on the articulated robot-based and gantry-based LMD systems are a TWIN PF 2/2-MF by GTV Verschleißschutz GmbH (Luckenbach, Germany) and a TWIN 10 C by Sulzer Metco AG (Wohlen, Switzerland). Even though separate companies manufacture these two devices, they both operate on the same rotating disk principle. The powder feeder is also in charge of the process gases, specifically the carrier and shielding gases, both of which were Argon.

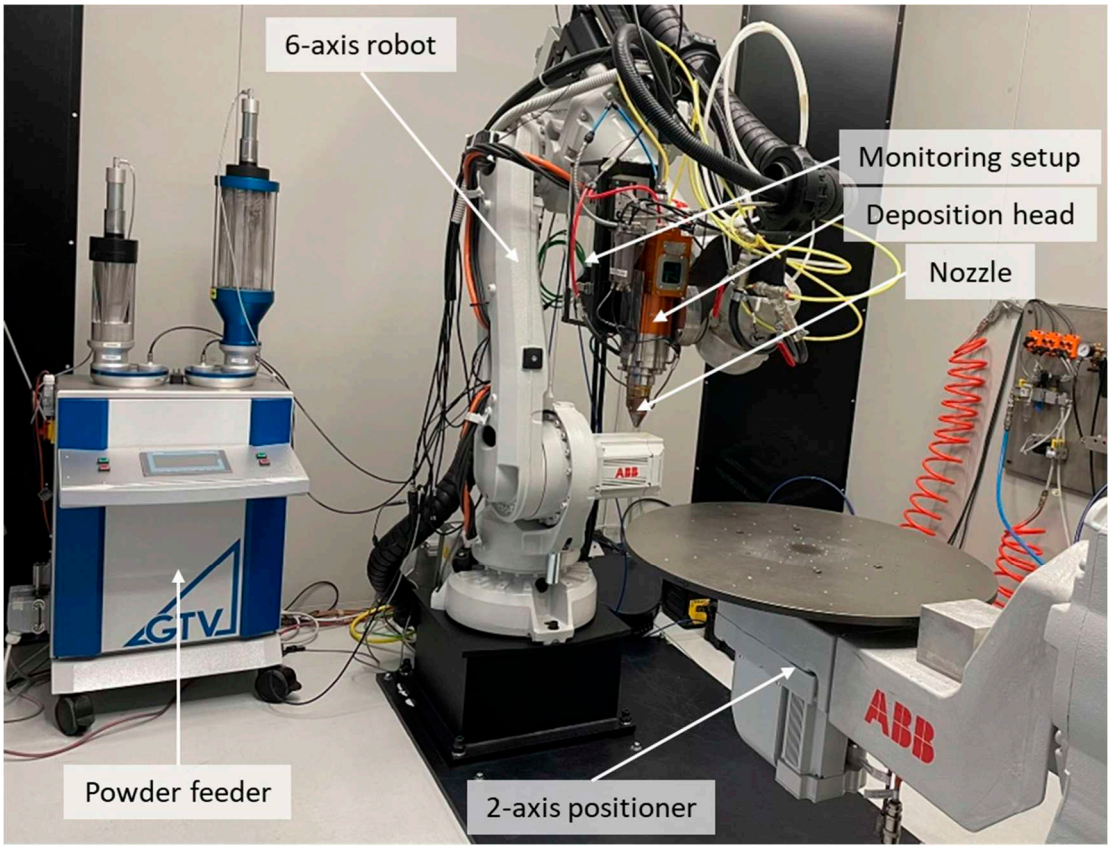

Figure 3. The eight-axis articulated robot based LMD system.

The fundamental difference between the two studied LMD machines, as stated previously, is the kinematics setup and size. The articulated robot-based system is comprised of an IRB 4600 45 six-axis articulated robot and an IRBP A 250-2 axis positioner from ABB Ltd. (Västerås, Sweden). The robot holds and moves the deposition head while the positioner manipulates the substrate for deposition using a flat steel circular table with a diameter of 700 mm. The CNC gantry-based system is composed of a three-axis gantry and a two-axis positioner, both of which were designed and built by SM Systems S.r.l (Torre Canavese,

Italy). The deposition head is mounted on the three-axis gantry, and the substrate is handled by the positioner. The positioner is furnished with a 2000 mm diameter steel flat circular table. Two cylindrical build volumes distinguish the two machines: Ø700 × 900 mm for the BLM GROUP machine, Ø2000 × 1500 mm for the SM Systems one. Notice that these build volumes consider only the positioner table surface as a building platform. Furthermore, the ABB positioner has a maximum payload of 250 kg, whereas the SM System machine can hold up to 1500 kg. NX by Siemens PLM Software (Plano, TX, USA) was used to program the tool path and generate the RAPID code to operate the robot-based machine, whereas hyperMILL by OPEN MIND Technologies AG (Wessling, Germany) was used to drive the gantry-based machine, which uses the G-code.

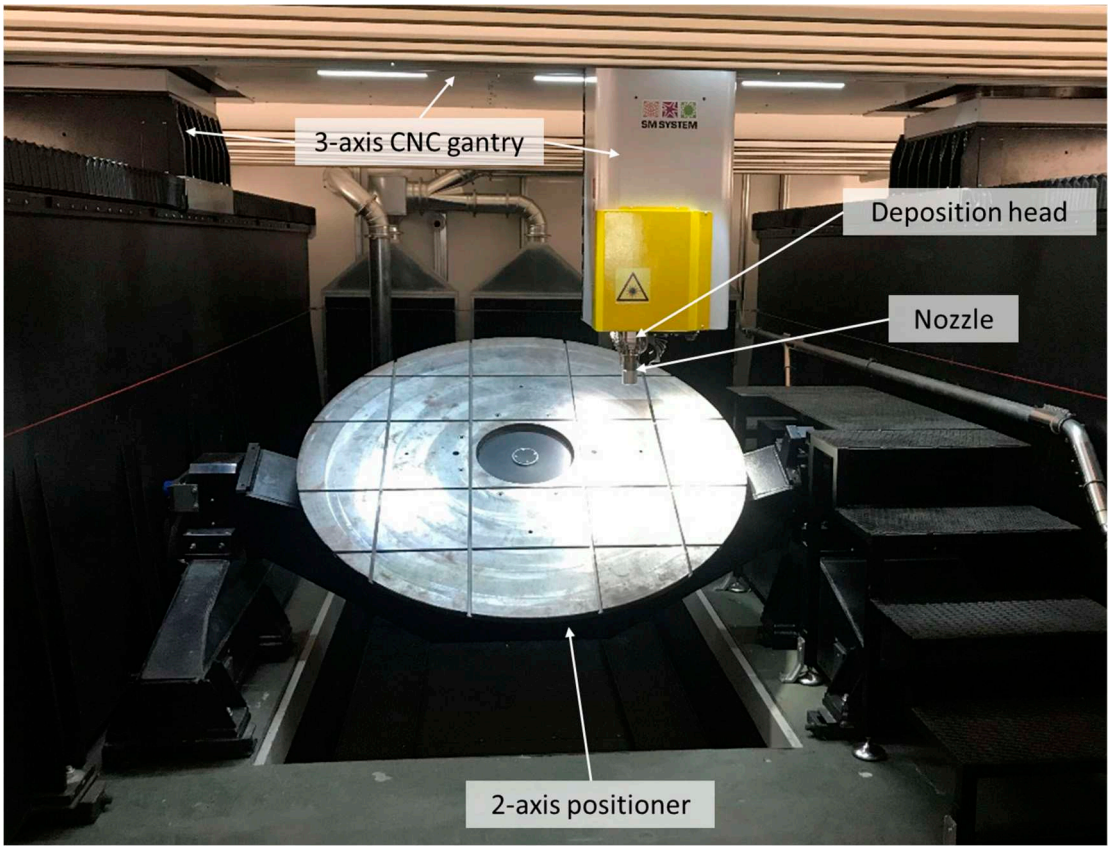

Figure 4. The five-axis CNC gantry-based LMD system.

2.3. Case Study Definition and Realization

To compare the two machines in their capability of producing a large-scale component, a realistic axisymmetric component of a gas turbine was chosen as the case study. The original component was resized to meet both machines' build sizes and to reduce total deposition time. Figure 5 depicts a 3D model of the scaled component used to realize the tool trajectories as well as a vertical section with its dimensions.

Starting from the bottom, the component is made up of three major sectors that reflect various deposition modalities:

- Sector A (standard vertical deposition): the base of the component is realized keeping the substrate horizontal;
- Sector B (multi-axis deposition): the substrate tilts following the curvature of the main body of the component, maintaining a flat working plane in the deposition area;
- Sector C (deposition on already deposited component): the substrate tilts at 90° to allow the deposition of a flange on the outer side of the already deposited component.

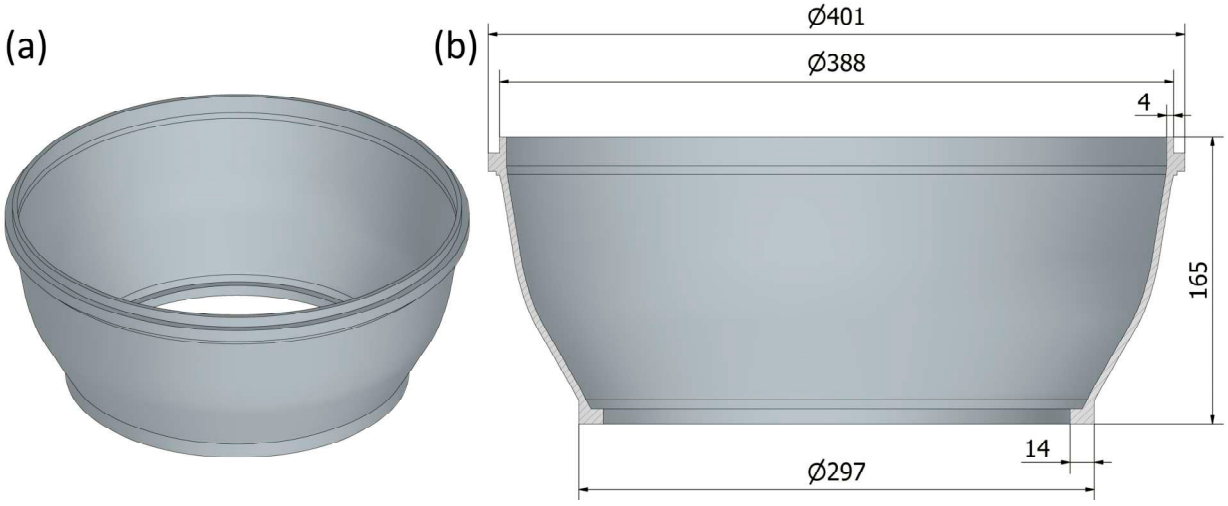

Figure 5. (**a**) The 3D model of the scaled component and (**b**) a vertical section with its main dimensions.

The substrate tilting allows the deposition head to be fixed in a vertical position and always deposited on a horizontal surface. This solution is helpful because it prevents the molten pool from dropping on the sides of the component during the construction of the sloping walls [29]. Furthermore, the deposition head in the gantry-based machine can only translate but not rotate, making this the sole possible method for component realization. As a result, the slicing operation adapts to the slope of the component wall, ensuring that the building orientation is always normal to the layers and vertical during deposition. Figure 6 depicts a simplified illustration of the deposition of the three sectors.

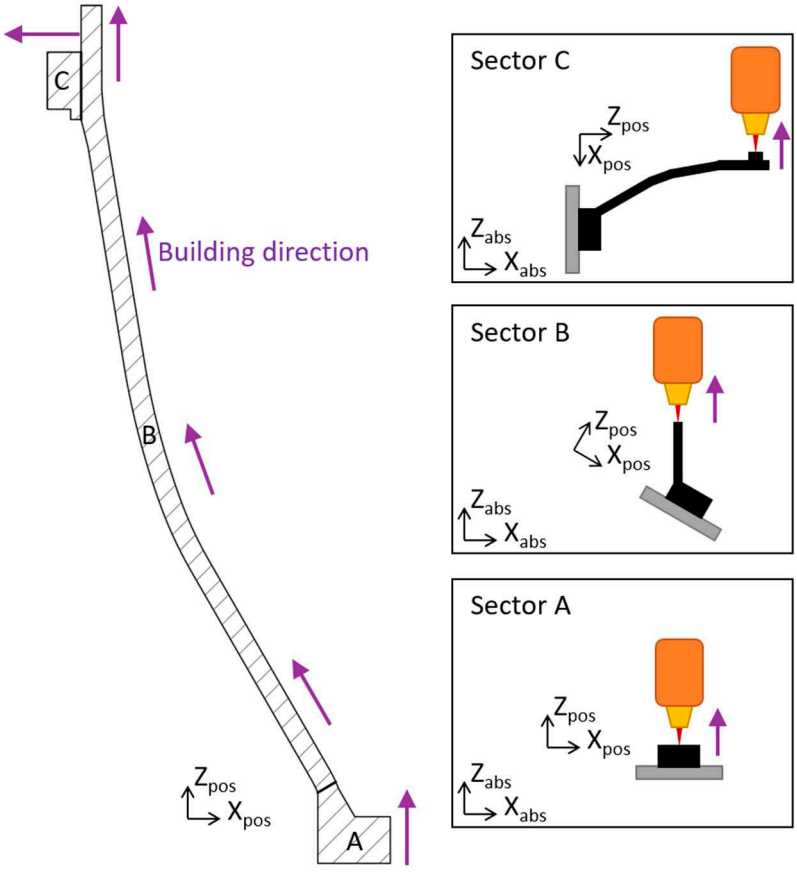

Figure 6. Illustration of the deposition strategy (purple arrows indicate the building directions).

For every layer, the scanning method is made up of internal and external single circular contours connected by a spiral. The sequence is repeated for each layer (inward and outward), and the rotation direction is always the same. As a result, the realization of the three sectors of the component can be completed with continuous deposition, eliminating the requirement to switch the laser on and off at each layer change. Because no beam compensation was used, the laser beam center crossed the whole thickness of the component. In this case, the real thickness of the deposited component would be more than the nominal thickness by approximately the width of a deposited track. The decision was made to meet the necessity for depositing stock material that would need to be removed by machining following deposition while keeping a functional component in mind. The scanning approach scheme is depicted in Figure 7.

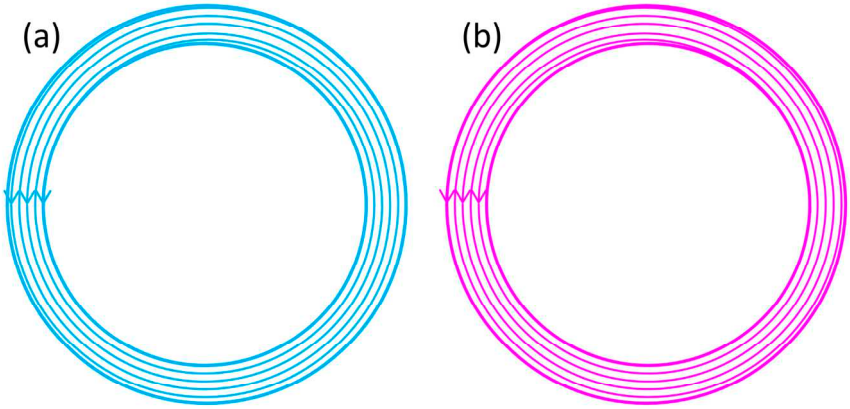

Figure 7. The adopted scanning strategy for (**a**) even and (**b**) odd layers.

A single M16 screw in the center of the bulk substrate, on which the component is formed, connects it to the positioner table. All relative linear motions between the substrate and the table are constrained by this fixture. The addition of lateral blockages inhibits the relative rotation of the substrate along the normal axis of the positioner (Z_{pos}). The substrate is well linked to the positioner in this fixture design, although its bending around is unrestricted. This solution was chosen for the investigation of substrate and component deformations during deposition. Indeed, due to residual tensions, the component tends to shrink in the circumferential direction, resulting in radial shrinkage as well [30]. As a result, the substrate should bend towards the center. Because neither of the positioner tables has a threaded hole in the center, two interface plates were created to link the substrates to the two positioner tables of the two machines. Because the laser source, optical, and powder feeding configurations of the two machines are similar, the same set of process parameters (laser power, laser spot diameter, scan speed, powder feed rate, shielding gas flow rate, carrier gas flow rate, standoff distance, hatch spacing, and Z step) are used on both machines. Because of this, any differences in geometrical accuracy and deformation of deposited components can be attributed to the kinematic mechanisms of the two machines. Furthermore, a standard set of process parameters (reported in Table 2) was used, resulting in a productivity/deposition rate of roughly 0.3 kg/h but a low heat load on the component since a relatively low level of laser power (875 W) was delivered on a large laser spot diameter (2.4 mm). The same laser spot was set on the two machines by adjusting the distance between the collimation lens and the process fiber outlet in the deposition heads. The operation was conducted with the aid of a Beamage Series USB 3.0 beam profiling camera by Gentec (Quebec City, QC, Canada) to measure the laser spot diameter on the working plane. The scan speed was also limited to reduce the molten pool vibrations and instabilities. The initial standoff distance was set to 8 mm at the beginning of the process, but it should be noticed that it may naturally slightly vary during the deposition due to the component growing more or less than expected. The hatch spacing is the spiral pitch in the scanning approach employed. Single tracks were produced on both machines using

the chosen set of process parameters as preliminary research to examine the concordance of the depositions. The tracks were cut transversally and polished to reveal their cross sections. The images were captured using an optical microscope, and the width, height, and cross-section area were calculated using ImageJ software [31].

Table 2. The set of process parameters used on the two machines.

Laser power, [W]	875
Laser spot diameter, [mm]	2.4
Scan speed, [mm/s]	10
Initial standoff, [mm]	8
Powder feed rate, [g/min]	9

2.4. Geometrical Characterization

The same component was deposited on both machines under the same conditions (building strategy, process parameters, substrate fixture, etc.).

During the depositions, ten pauses were taken at specific points, typically every 16 layers. The distance between the top surface of the substrate and the positioner table was measured with a caliper in eight specific positions along the perimeter of the substrate: at the four corners and at the four midpoints of the substrate sides, during the ten pauses, and after the deposition competition. The measured heights are made up of the substrate thickness (which is assumed to be constant) and its deformation, which is caused by the residual stress of the component. Once in place on the positioner tables, initial height measurements of the two substrates in the eight considered places were taken and utilized as the baseline to calculate cumulative deformation at the various pauses. Furthermore, the current deformation increment is calculated by subtracting the cumulative deformation at each pause from the previously measured value. The distance between the sampling locations and the center of the substrate, which is the sole section of it that is attached to the positioner table and cannot move, is used to standardize the readings. The residual stress action on the substrate and the component itself can be evaluated by assessing the cumulative deformation and deformation increments at each planned stop. This information aids in the interpretation of the outcomes of the 3D scanning procedure. Figure 8 illustrates the positions of the pauses taken during the deposition phase to measure the substrate height, as well as a representative scheme of the taken measurement and the probing spots on the substrate perimeter.

Following deposition, the two components were scanned with an EDGE ScanArm by FARO Technologies Inc. (Lake Mary, FL, USA), yielding a 3D reconstruction of the actual deposited components. The components were not removed from the substrate. The two resulting 3D models were then dimensionally compared to the original CAD file, with the CAD file aligned to the 3D acquisitions using the substrate top surface surrounding the component base and the component axis of symmetry. This comparison highlights geometrical inaccuracies and distortions between the programmed tool path and the actually deposited component. In addition, the two 3D acquisitions were compared, revealing variances between the two machines. Four sections were also virtually sliced so that the variations between the designed and deposited components could be easily identified. By intersecting the component scans and CAD file with two vertical and orthogonal planes centered on the component axis, the four sections were obtained (Figure 9). These analyses were conducted on PolyWorks Inspector, by InnovMetric Software Inc. (Quebec City, QC, Canada).

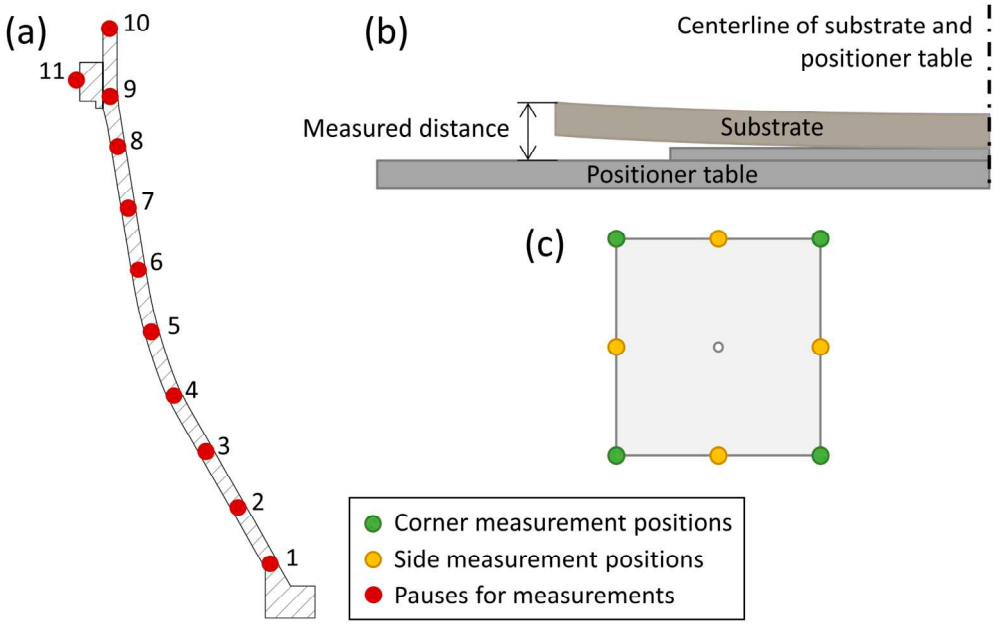

Figure 8. (**a**) positions of the pauses during the component realization phase for measuring the distance between the top surface of the substrate and the positioner table; (**b**) lateral view of the mounted and deformed substrate with the scheme of the measurement procedure; (**c**) top view of the substrate with the positions of the height measurement points along the substrate perimeter.

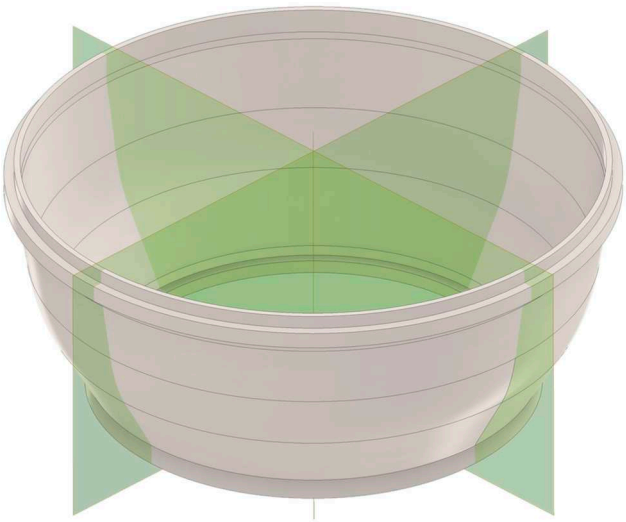

Figure 9. Position of the two section planes.

3. Results

Figure 10 shows the cross-sections of two single tracks produced on the two considered machines using the same set of process parameters that were later used to realize the case study. Table 3 summarizes the geometrical properties of the two deposited tracks. The two cross sections match, indicating that the depositions made with the two machines using the identical set of process settings are equivalent. As a result, the remarkable similarity between the two machines in terms of the laser source, optical, and powder feeding arrangement resulted in very comparable deposition properties. This ensures that any possible geometrical discrepancy between the two deposited components may be attributed to the kinematics of the two machines, which are vastly different.

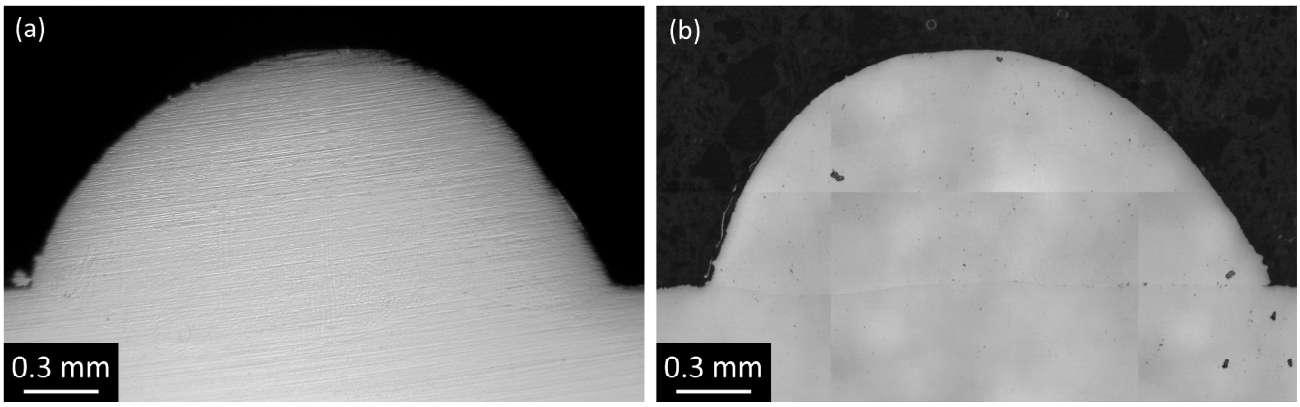

Figure 10. Cross sections of the single tracks realized with the same set of process parameters (**a**) on the articulated robot-based LMD machine and (**b**) on the gantry-based LMD machine.

Table 3. Geometrical characteristics of the two tracks deposited with the two machines (mean ± standard deviation).

Machine	Width [mm]	Height [mm]	Cross-Section Area [mm^2]
Articulated robot-based	2.35 ± 0.01	0.95 ± 0.01	1.58 ± 0.02
Gantry-based	2.27 ± 0.01	0.94 ± 0.01	1.55 ± 0.02

Figure 11 portrays the two realized components, one deposited with the articulated robot-based system and the other with the CNC gantry-based system. The pictures were acquired directly after the deposition and cleaning phases, with the components and substrates still linked to the positioner table via the interface plates (that is not visible in the articulated robot-based system since it is narrower than the substrate).

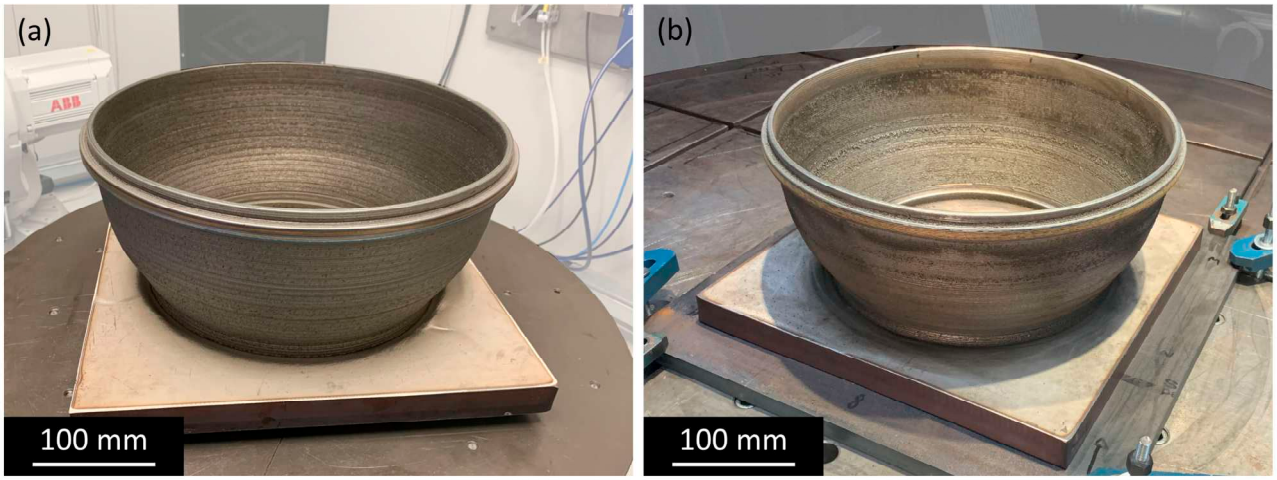

Figure 11. The deposited components (**a**) deposited with the articulated robot-based system and (**b**) with the gantry-based system.

Figure 12 shows the normalized cumulative deformations and normalized deformation increments measured during the two depositions. These results are obtained by averaging the measurements taken at the four corners and four sides after normalization based on their distance from the substrate center. Analyzing the deformation of the two substrates through the two abovementioned graphs, it appears that the substrates deform significantly at the start of the deposition. Indeed, the greatest deformation was observed in both depositions during the first stop. After the third pause, the deformation of the substrates halted, and no substantial alterations were recorded, only oscillations due to measurement

uncertainty. Another thing to notice when looking at these graphs is the exact similarity of the deformations of the two substrates during the two depositions on the two machines. The graphs are substantially overlapping, indicating that the substrates act similarly: both deform significantly at the start of the deposition and do not deform after a few layers.

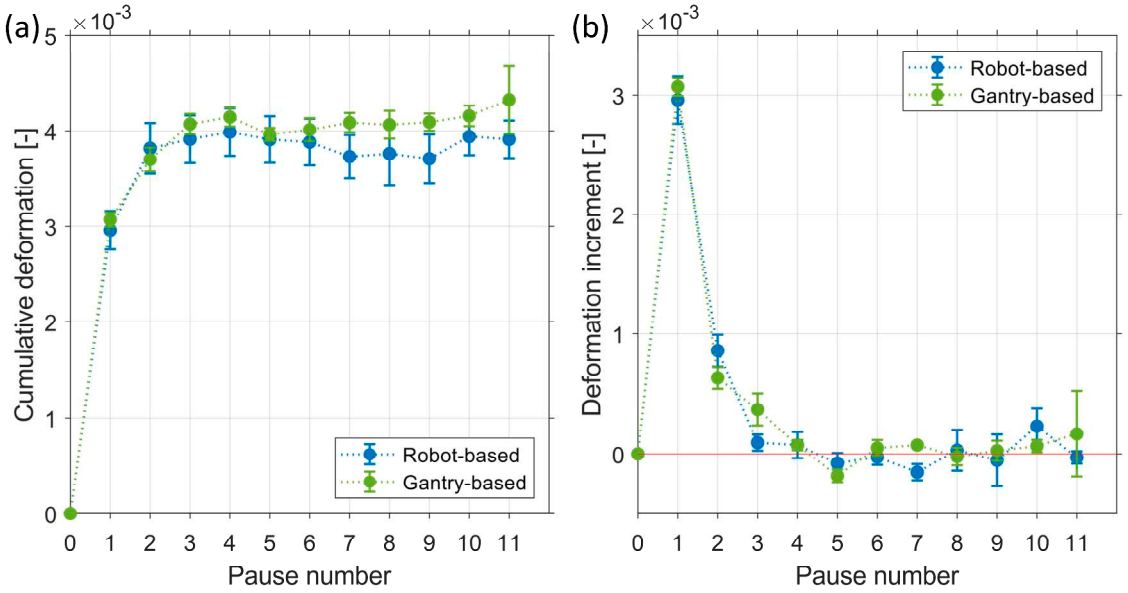

Figure 12. (**a**) Average normalized cumulative deformations and (**b**) average deformation increments of the substrates of the two depositions at the various pauses. The error bars represent the standard error of the mean.

Figure 13 displays the dimensional difference between the two 3D scans of the realized components and the original CAD file. According to a basic analysis of the pseudo-colored surfaces, both components are distorted similarly and are obviously bent towards the part centerline at the top.

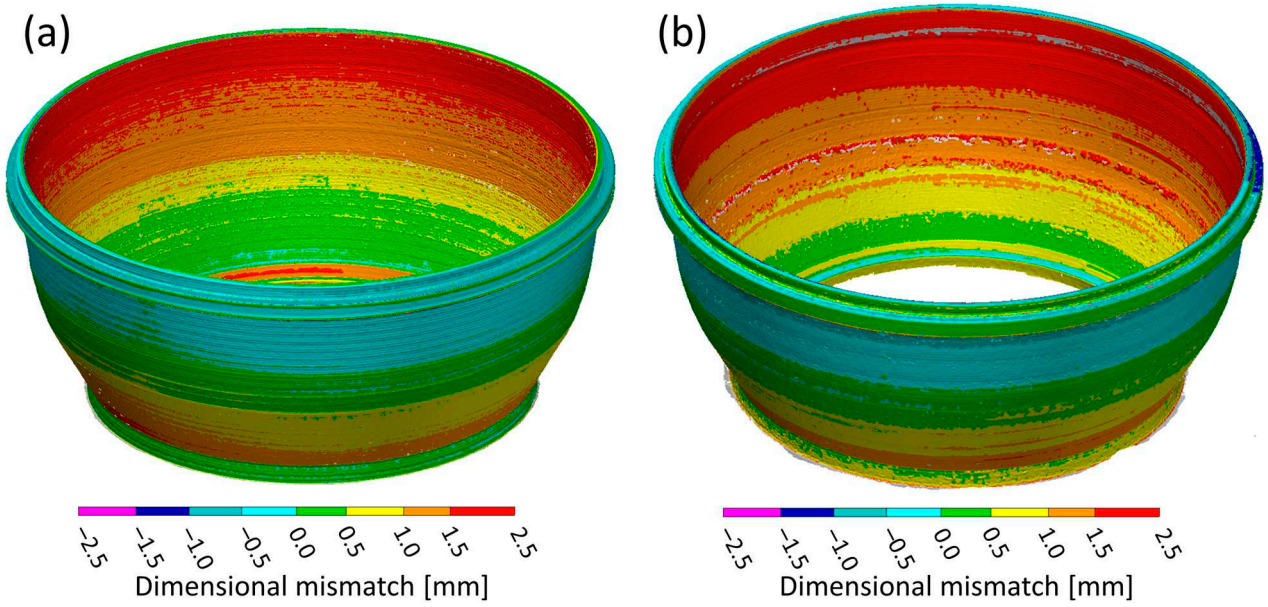

Figure 13. Dimensional mismatch between the 3D scan of the component realized with (**a**) the articulated robot-based system or (**b**) the gantry-based system and the original CAD file.

Figure 14 compares the four scan sections to the sections of the CAD file. The same comparisons are made in Figure 15, with the measured dimensional disparity between the 3D

scans and the CAD file shown in pseudo colors. Both realized components are thicker than the planned model. This was to be expected, and it is explained by the lack of use of beam radius compensation. As a result, the deposited component is overall thicker than the planned one by a factor near the deposited track width, as shown in Table 3. Both components are nearly identical to the nominal design at the base (sector A in Figure 8a), where the alignment method between the 3D scan and the nominal CAD is also performed. Only the component created using the articulated robot-based system exhibits a minor overgrowth in this first region, where the wall thickness is decreasing. As one ascends sector B, it is evident that the deposited components on both machines are gradually bending towards the center due to residual tensions that are typical of the process. The internal surface difference between the deposited and designed components is approximately 2.5 mm in the upper section, while the two external surfaces are nearly matching.

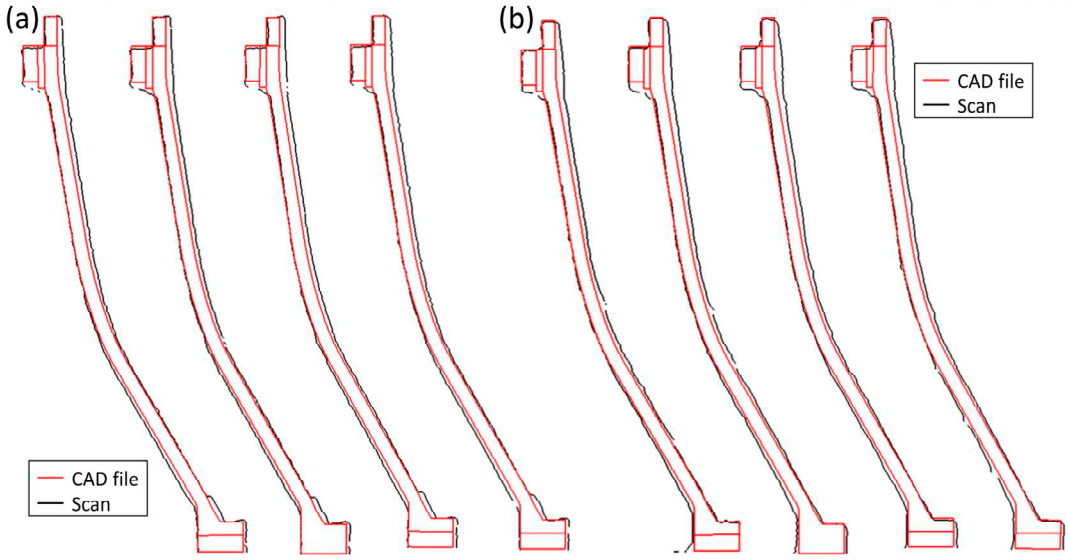

Figure 14. Comparison between the sections of the scan of the component realized with (**a**) the articulated robot-based system or (**b**) the gantry-based system and the corresponding sections of the original CAD file.

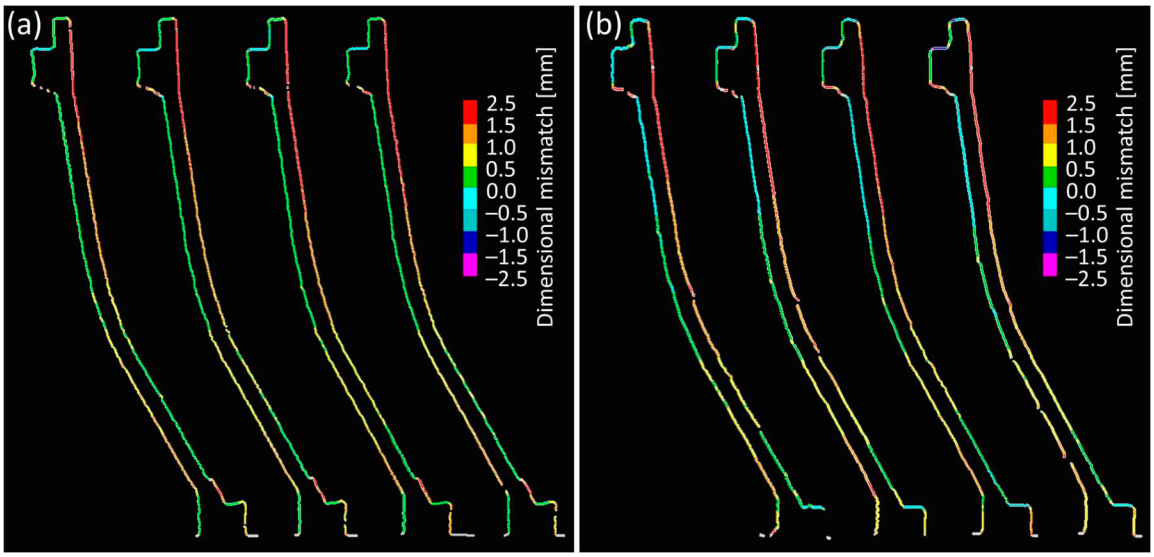

Figure 15. Dimensional mismatch between the 3D scan of the component realizes with (**a**) the articulated robot-based system or (**b**) the gantry-based system and the original CAD file at four vertical sections.

The 3D scans of the two deposited components were also compared to each other, as shown in Figure 16. The differences between the two parts are limited. The component deposited with the CNC gantry-based LMD machine is slightly more bent to the center with respect to the other one. Furthermore, the pauses in sector B corresponding to variations in curvature are more visible in the former scan than in the latter (also considering Figure 13). Moreover, there is a variation in total height between the two components: the component realized using the articulated robot-based machine is slightly taller than the other. The geometrical mismatch between the two components is small overall.

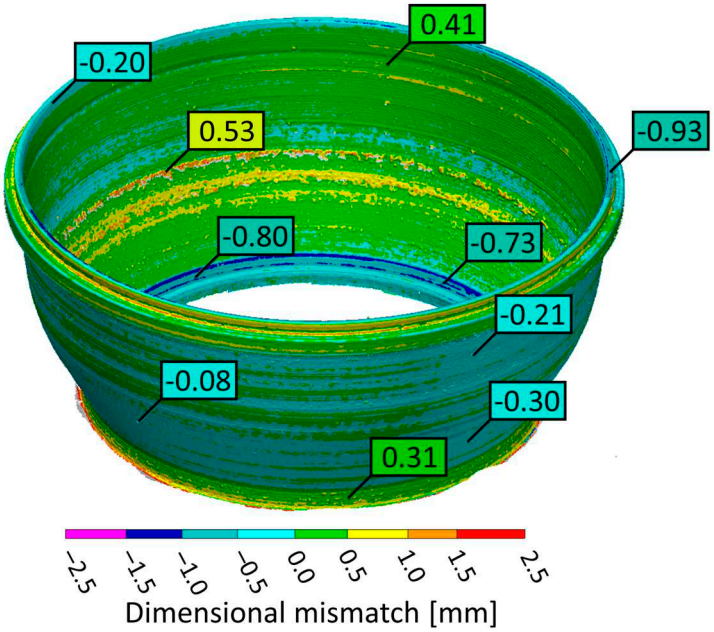

Figure 16. Dimensional mismatch between the 3D scan of the component realized with the CNC gantry-based system and the 3D scan of the component realized with the articulated robot-based one.

4. Discussion

As previously stated, one of the major challenges that the LMD process must overcome to gain traction for industrialization in fields such as aerospace, oil and gas, and construction is the generally higher cost per part compared to other conventional manufacturing technologies [1]. Indeed, the initial investment of buying an LMD system is difficult to amortize because of the limited series manufacturing that these machines are typically destined for. There are numerous approaches to making an LMD system more inexpensive, which can all be summed up as improving overall process sustainability. A requirement for sustainability is that the process should be accurate and reproducible in the realization of the designed components, avoiding the need for extensive preliminary testing and limiting the quantity of produced scrap components. As a result, LMD machine manufacturers typically provide solutions based on CNC gantry or cartesian kinematics, which are generally more precise and robust than articulated robot-based systems, but much more expensive and less flexible [21].

The investigation in this research aims to shed light on this aspect of LMD by assessing the performances in terms of geometrical accuracy of two machines with identical optical and material feeding configurations but different kinematic mechanisms and sizes and comparing them. For this scope, an oil and gas case study was chosen, and the designed component was built on both machines under identical conditions (process parameters, materials, fixture configuration, and pauses for measurements). In order to avoid over-constraints that could threaten the outcome of the builds or represent a dissimilarity between the two builds, the component was given the most freedom of deformation possible.

The analogy between the geometry and internal appearance of tracks deposited on the two machines and with the same process parameters is assessed using the cross sections shown in Figure 10. When the same set of process parameters is used, the width, height, and cross-section area of the two measured tracks match. Based on this verification, it is reasonable to assume that the analysis of geometrical inaccuracies performed via 3D scan can highlight differences in the builds due to the different kinematic configurations of the two machines.

The substrate deformations during the builds were measured at predetermined time stamps. This analysis provides a history of the residual stress action on the substrate and improves the interpretation of the results of the 3D scans of the two components, which were only performed at the end of the depositions. Figure 12 clearly shows that residual stresses cause component distortion only up to a certain number of layers. The substrate does indeed deform only for the first few layers of the depositions, bending towards the center of the deposition, as expected [32]. The substrates are no longer deformed after approximately 34 layers. The substrate deformation, which is an index of the residual stresses induced by the process, is related to the process parameters chosen. Because the process parameters on both machines are the same, the deformation of the two substrates is expected to be similar. Figure 12 shows that the graphs of the substrate deformations during the two builds are highly overlapping, confirming the hypothesis.

The 3D scans of the two deposited components were performed after the second deposition while the component was still attached to the substrate. This decision was made to make the measurements and their interpretation more understandable. Indeed, removing the substrate would result in a redistribution of residual stresses and a considerable change in the shape of the component. The focus of the proposed work is not the analysis of the deformations themselves but rather the comparison of the two LMD machines in terms of geometrical accuracy. Consequently, it was convenient to keep the components attached to their substrate during acquisition, which was also advantageous for the scan alignment procedure. According to Figures 13–15, the component is progressively contracting, moving from the bottom to the top, and it is bending toward its center axis. The presence of the bulk substrate, which absorbs residual stresses, causes less deformation at the base of the component. As previously explained in relation to Figure 12, the influence of the substrate decreases as the layers ascend. This corresponds to the visible bending of the component. The geometrical distortion is so significant that the outer surface of the deposited part overlaps with one of the CADs at the top of the component: there is no machining allowance here, and the stock material on the inner surface is excessive. Residual stresses are always present in the DED LB process and distort the component during deposition. Heat treatments on the component can relieve residual tensions. However, after being removed from the substrate and heat treatments are applied, the final output will not match the planned CAD file. A common practice is to deposit and treat the component once, then measure the distortions with a 3D scan and create a new CAD file correcting for the component deformations, expanding it where it is shrunk, and downsizing it where it is larger. Another method for predicting deformations is to do simulations of the heat cycles of the deposition [32,33].

The comparison of the two deposited components confirms that there are no major differences when analyzing the capability of the two machines of accurately depositing the chosen component. The deformation behavior of the two realized parts does match. The component realized in the articulated robot-based LMD machine has only a small overgrowth. However, because of the self-regulation phenomenon typical of the process, overgrowth concerns are reduced and do not propagate during the builds [34]. Further to that, the component produced by the gantry-based machine is rougher on its inner wall in some positions than the component produced by the articulated robot-based machine: there is material accumulation in the central region of sector B, where the slope of the wall varies between 30 deg and 9 deg. The increased roughness is caused by sintered material on the side of the component. This imperfection can be removed using surface cleaning

procedures or by machining when the allowance is removed. These two considerations indicate that, even though the machines are remarkably similar in many ways (laser source, optics, and powder delivery system) and the deposited single tracks are equivalent, the machines perform slightly differently. However, these two aspects (overgrowth of the component realized with the articulated robot-based system and sintered material on the inner side of the component realized with the gantry-based system) cannot be attributed to the kinematics of the two machines but are most likely related to minor differences in the laser source, optics, and powder delivery systems, or to different wear states of them. As a result, when only the actual deformation state of the two components is considered, there are no significant disparities that can be attributed to the two different kinematics of the two machines, indicating that increased accuracy of CNC machines is not required when dealing with LMD of large axisymmetric components.

5. Conclusions

Two nearly identical large-scale LMD machines in terms of the laser source, optics, and powder delivery configuration were compared in the realization of an oil and gas case study. The axis configuration differs significantly between the two machines: one is an eight-axis articulated robot, whereas the other uses a five-axis CNC gantry architecture. On both machines, the same axisymmetric large component was fabricated using the same conventional set of process parameters. In order to compare the geometrical accuracy of the two machines, the deposited components were 3D scanned and compared to the original CAD file. The two 3D scans were also compared to better assess the performance differences between the two machines.

- As a result of residual stresses caused by the process, the deposited components deformed toward their centerlines, diverging from the designed part. They both distorted similarly, with no discernible difference between them;
- The geometrical accuracy comparison between the two deposited components revealed no significant discrepancy that could be attributed to the distinct kinematic architecture of the two machines. In the chosen application, the greater accuracy and precision of the CNC gantry system over the articulated robot is not essential.

In conclusion, while there were differences in the kinematic architecture of the two large-scale LMD machines used in this study, the comparison of their performance in terms of geometrical accuracy showed no significant discrepancy in the analyzed case study, which is axisymmetric and with a remarkable thickness. Even though the hypothesis is verified on the chosen geometry, this is representative of many components that are typical of the oil and gas field. For this reason, the findings are extendable and applicable to many other elements.

For this scenario, the decision between the two systems is not crucial because both machines provided comparable results. Yet, the two systems have distinct advantages and disadvantages. The articulated robot provides greater versatility and can perform a variety of tasks. Furthermore, if the necessity to realize more complicated structures arises, the increased number of axes is advantageous to freeform manufacturing. Finally, relatively low-cost or articulated robots are significant when cost reduction is desired. For these reasons, an articulated robot is clearly the best option in a research setting. On the other hand, a CNC machine is preferred when the easiness of programming is required, as is the robustness and reliability of the system. Hence, this is more applicable to an industrial and production environment. However, it should be considered that the cost of a CNC gantry system may quickly rise when going up with dimensions.

Further developments of this work may be related to the examination of more complicated and non-axisymmetric structures than the one chosen for this work. Finally, similar research should be conducted on additional sets of process parameters that increase the deposition rate, as these typically increase the heat input to the material.

Author Contributions: Conceptualization, S.M., F.C., G.M. and V.F.; methodology, S.M., F.C., G.M. and V.F.; software, S.M.; validation, S.M.; formal analysis, S.M.; investigation, S.M., F.C. and G.M.; resources, G.M. and M.G.; data curation, S.M.; writing—original draft preparation, S.M.; writing—review and editing, S.M. and B.P.; visualization, S.M.; supervision, B.P.; project administration, M.G. and B.P.; funding acquisition, M.G. and B.P. All authors have read and agreed to the published version of the manuscript.

Funding: This research received no external funding.

Institutional Review Board Statement: Not applicable.

Informed Consent Statement: Not applicable.

Data Availability Statement: Not applicable.

Acknowledgments: Nuovo Pignone Tecnologie S.R.L. (Baker Hughes) is acknowledged for granting the industrial PhD scholarship which made this research possible, as well as their extensive knowledge and support. We gratefully acknowledge BLM Group for providing the robotic LMD system used in this study, as well as their technical support and assistance. We are deeply grateful for the contributions of both companies and their commitment to advancing research in this field.

Conflicts of Interest: The authors declare no conflict of interest.

References

1. Tarancón, A.; Esposito, V.; Torrell, M.; Vece, M.D.; Son, J.S.; Norby, P.; Barg, S.; Grant, P.S.; Vogelpoth, A.; Linnenbrink, S.; et al. 2022 roadmap on 3D printing for energy. *J. Phys. Energy* **2022**, *4*, 011501. [CrossRef]
2. Langefeld, B. *Sustainability in Additive Manufacturing*; Roland Berger GMBH: Munich, Germany, 2022; p. 9.
3. Blakey-Milner, B.; Gradl, P.; Snedden, G.; Brooks, M.; Pitot, J.; Lopez, E.; Leary, M.; Berto, F.; Plessis, A.D. Metal additive manufacturing in aerospace: A review. *Mater. Des.* **2021**, *209*, 110008. [CrossRef]
4. Izadi, M.; Farzaneh, A.; Mohammed, M.; Gibson, I.; Rolfe, B. A review of laser engineered net shaping (LENS) build and process parameters of metallic parts. *Rapid Prototyp. J.* **2020**, *26*, 1059–1078. [CrossRef]
5. Gibson, I.; Rosen, D.; Stucker, B. Directed Energy Deposition Processes. In *Additive Manufacturing Technologies: 3D Printing, Rapid Prototyping, and Direct Digital Manufacturing*; Gibson, I., Rosen, D., Stucker, B., Eds.; Springer: New York, NY, USA, 2015; pp. 245–268. [CrossRef]
6. Gradl, P.; Tinker, D.C.; Park, A.; Mireles, O.R.; Garcia, M.; Wilkerson, R.; Mckinney, C. Robust Metal Additive Manufacturing Process Selection and Development for Aerospace Components. *J. Mater. Eng. Perform.* **2022**, *31*, 6013–6044. [CrossRef]
7. Jiang, J.; Newman, S.T.; Zhong, R.Y. A review of multiple degrees of freedom for additive manufacturing machines. *Int. J. Comput. Integr. Manuf.* **2021**, *34*, 195–211. [CrossRef]
8. Bhatt, P.M.; Malhan, R.K.; Shembekar, A.V.; Yoon, Y.J.; Gupta, S.K. Expanding capabilities of additive manufacturing through use of robotics technologies: A survey. *Addit. Manuf.* **2020**, *31*, 100933. [CrossRef]
9. Siciliano, B.; Khatib, O. (Eds.) *Springer Handbook of Robotics*; Springer International Publishing: Cham, Switzerland, 2016. [CrossRef]
10. Ye, C.; Yang, J.; Ding, H. High-accuracy prediction and compensation of industrial robot stiffness deformation. *Int. J. Mech. Sci.* **2022**, *233*, 107638. [CrossRef]
11. Wang, W.; Guo, Q.; Yang, Z.; Jiang, Y.; Xu, J. A state-of-the-art review on robotic milling of complex parts with high efficiency and precision. *Robot. Comput. Integr. Manuf.* **2023**, *79*, 102436. [CrossRef]
12. Wu, K.; Kuhlenkoetter, B. Dynamic behavior and path accuracy of an industrial robot with a CNC controller. *Adv. Mech. Eng.* **2022**, *14*, 16878132221082868. [CrossRef]
13. Bremer, J.; Walderich, P.; Pirch, N.; Schleifenbaum, J.H.; Gasser, A.; Schopphoven, T. Effects of path accuracy on additively manufactured specimens by laser material deposition using six-axis robots. *J. Laser Appl.* **2021**, *33*, 012045. [CrossRef]
14. Taşdemir, A.; Nohut, S. An overview of wire arc additive manufacturing (WAAM) in shipbuilding industry. *Ships Offshore Struct.* **2021**, *16*, 797–814. [CrossRef]
15. Flynn, J.M.; Shokrani, A.; Newman, S.T.; Dhokia, V. Hybrid additive and subtractive machine tools—Research and industrial developments. *Int. J. Mach. Tools Manuf.* **2016**, *101*, 79–101. [CrossRef]
16. Bandari, Y.K.; Williams, S.W.; Ding, J.; Martina, F. Additive Manufacture of Large Structures: Robotic or CNC Systems? In Proceedings of the 2015 International Solid Freeform Fabrication Symposium, Austin, TX, USA, 10–12 August 2015; Available online: https://repositories.lib.utexas.edu/handle/2152/89305 (accessed on 31 December 2022).
17. Brunete, A.; Gambao, E.; Koskinen, J.; Heikkilä, T.; Kaldestad, K.B.; Tyapin, I.; Hovland, G.; Surdilovic, D.; Hernando, M.; Bottero, A.; et al. Hard material small-batch industrial machining robot. *Robot. Comput.-Integr. Manuf.* **2018**, *54*, 185–199. [CrossRef]
18. Feucht, T.; Waldschmitt, B.; Lange, J.; Erven, M. Additive manufacturing of a bridge in situ. *Steel Constr.* **2022**, *15*, 100–110. [CrossRef]

19. Raut, L.P.; Taiwade, R.V. Wire Arc Additive Manufacturing: A Comprehensive Review and Research Directions. *J. Mater. Eng. Perform* **2021**, *30*, 4768–4791. [CrossRef]
20. Watson, N.D.; Meisel, N.A.; Bilén, S.G.; Duarte, J.; Nazarian, S. Large-Scale Additive Manufacturing of Concrete Using a 6-Axis Robotic Arm for Autonomous Habitat Construction. In Proceedings of the 2019 International Solid Freeform Fabrication Symposium, Austin, TX, USA, 12–14 August 2019. [CrossRef]
21. Puzatova, A.; Shakor, P.; Laghi, V.; Dmitrieva, M. Large-Scale 3D Printing for Construction Application by Means of Robotic Arm and Gantry 3D Printer: A Review. *Buildings* **2022**, *12*, 2023. [CrossRef]
22. Lehmann, T.; Rose, D.; Ranjbar, E.; Ghasri-Khouzani, M.; Tavakoli, M.; Henein, H.; Wolfe, T.; Qureshi, A.J. Large-scale metal additive manufacturing: A holistic review of the state of the art and challenges. *Int. Mater. Rev.* **2022**, *67*, 410–459. [CrossRef]
23. Alhijaily, A.; Kilic, Z.M.; Bartolo, A.N.P. Teams of robots in additive manufacturing: A review. *Virtual Phys. Prototyp.* **2023**, *18*, e2162929. [CrossRef]
24. Tao, B.; Zhao, X.; Ding, H. Mobile-robotic machining for large complex components: A review study. *Sci. China Technol. Sci.* **2019**, *62*, 1388–1400. [CrossRef]
25. Urhal, P.; Weightman, A.; Diver, C.; Bartolo, P. Robot assisted additive manufacturing: A review. *Robot. Comput. Integr. Manuf.* **2019**, *59*, 335–345. [CrossRef]
26. Sanandiya, N.D.; Vijay, Y.; Dimopoulou, M.; Dritsas, S.; Fernandez, J.G. Large-scale additive manufacturing with bioinspired cellulosic materials. *Sci. Rep.* **2018**, *8*, 8642. [CrossRef] [PubMed]
27. Ji, W.; Wang, L. Industrial robotic machining: A review. *Int. J. Adv. Manuf. Technol.* **2019**, *103*, 1239–1255. [CrossRef]
28. *ASTM B637-18*; Specification for Precipitation-Hardening and Cold Worked Nickel Alloy Bars, Forgings, and Forging Stock for Moderate or High Temperature Service. B02 Committee; ASTM International: West Conshohocken, PA, USA, 2018. [CrossRef]
29. Gibson, B.T.; Mhatre, P.; Borish, M.C.; Atkins, C.E.; Potter, J.T.; Vaughan, J.E.; Love, L.J. Controls and process planning strategies for 5-axis laser directed energy deposition of Ti-6Al-4V using an 8-axis industrial robot and rotary motion. *Addit. Manuf.* **2022**, *58*, 103048. [CrossRef]
30. Turichin, G.; Zemlyakov, E.; Babkin, K.; Ivanov, S.; Vildanov, A. Analysis of distortion during laser metal deposition of large parts. *Procedia CIRP* **2018**, *74*, 154–157. [CrossRef]
31. Schneider, C.A.; Rasband, W.S.; Eliceiri, K.W. NIH Image to ImageJ: 25 years of image analysis. *Nat. Methods* **2012**, *9*, 671–675. [CrossRef]
32. Babkin, K.; Zemlyakov, E.; Ivanov, S.; Vildanov, A.; Topalov, I.; Turichin, G. Distortion prediction and compensation in direct laser deposition of large axisymmetric Ti-6Al-4V part. *Procedia CIRP* **2020**, *94*, 357–361. [CrossRef]
33. He, B.; Bi, C.; Li, X.; Wang, W.; Yang, G. Residual stresses and deformations of laser additive manufactured metal parts: A review. *Int. J. Mater. Form.* **2022**, *16*, 7. [CrossRef]
34. Donadello, S.; Furlan, V.; Demir, A.G.; Previtali, B. Interplay between powder catchment efficiency and layer height in self-stabilized laser metal deposition. *Opt. Lasers Eng.* **2022**, *149*, 106817. [CrossRef]